Turbulent Flow in Stirred Tanks

Part II: A Two-Scale Model of Turbulence

The two-scale turbulence concept is recommended for modeling the turbulence in a baffled vessel equipped with a Rushton-type turbine impeller. A three-equation isotropic turbulence model is proposed that employs the balance equations for: the kinetic energy of the large scale vortices; the kinetic energy of the inertial subrange eddies; and the dissipation rate of the small-scale turbulence. The energy transfer rate from the large-scale vortices is prescribed algebraically. Flow patterns are modeled by solving the transport equations for vorticity, stream function, and tangential momentum. The Reynolds stresses are modeled by means of the effective viscosity, based on the three-equation model of turbulence. The calculated profiles of the mean velocity at the tank wall agree with experimental data obtained in the same system by means of a Pitot tube.

Jiří Placek, L. L. Tavlarides and G. W. Smith
Department of Chemical Engineering
Syracuse University
Syracuse, NY 13244

Ivan Fořt
Department of Chemical and Food Process Equipment
Czech Technical University
Prague 6, Dejvice, Czechoslovakia

Introduction

Investigation of flow patterns in agitated vessels has received substantial attention as it represents a scale-up method for design of process apparatuses. Analytical models of fluid flow in tanks agitated by turbine impellers tend to oversimplify the flow situation due to the assumption of potential flow, and they usually require additional measurements within the system in question. In order to obtain reliable information about the macroflow patterns and the dead spaces within the tank, a model based on turbulent flow of the viscous fluid has to be used.

Developing a reliable flow model requires analysis of the system being considered. The proposed model must then be tailored to comply with the specific properties of the system. In this particular case, mathematical modeling of flow in mechanically agitated vessels represents a task complicated by the presence of three-dimensional asymmetric flow with highly intensive anisotropic turbulence. Further, boundary conditions specific for agitated systems must be introduced, and the instability of the numerical algorithm caused by the complexity of the system must be removed. Previous work (Placek and Tavlarides, 1985) established a model to describe turbulent flow in the impeller region for a Rushton-type turbine impeller. The method commonly used to predict velocity fields in turbulent flows is based upon the concept of turbulent viscosity, which is evaluated from the local values of overall kinetic energy of turbulence k and its dissipation rate ϵ. Balance equations of turbulent quantities must be solved simultaneously with the balance equations for mass and the mean momentum. Applied *ad hoc* to the mixing vessel, the k-ϵ model fails to give acceptable results of the turbulence parameters in mixing vessels, as indicated in the results of Platzer (1981). The approach applied here extends the classic k-ϵ model to include the turbulence energy scales k_p and k_T, where the former represents the production-scale vortices and the latter represents the inertial range eddies. The extended model is employed here to construct an algorithm for the computation of profiles of mean velocity, kinetic energy of turbulence, and dissipation rate of turbulence.

The model is compared with experimental data to evaluate the reliability of the numerical predictions. The numerical results for the mean velocity profiles in the wall region are compared with experimentally measured velocities for a laboratory-size vessel. The wall region presents many distinct advantages in measurements for validation of this model. These include verification of the secondary circulation, sufficiently high mean velocities for satisfactory accuracy, moderate levels of turbulence, and a check in the region where the assumption of axial symmetry may be violated. Wall measurements are preferable to impeller measurements because of large degrees of anisotropy

Part I of this paper was published in July, 1985.
Correspondence concerning this paper should be addressed to L. L. Tavlarides.
Jiří Placek is with Enzyme BioSystems Ltd., a unit of CPC International Inc., Argo, IL 60501.
Gregory W. Smith is with the Department of Chemical Engineering, University of Nebraska, Lincoln, NE 68588.

in the latter region. Also, impeller zone measurements would only serve to confirm already established boundary conditions.

The early development of k-ϵ models by Launder and Spalding (1972) has found wide acceptance for computing turbulent flows. Placek et al. (1978) employed these models for one of the first solutions for turbulent flow in mixing vessels employing Rushton turbine impellers. Platzer (1981) later applied these models to compute flows in a similar system. Harvey and Greaves (1982) also applied these models to predict turbulent flows in the mixing vessels they studied. Although these models successfully compute the mean flow quantities, second-order turbulence parameters such as turbulence kinetic energy and turbulence dissipation show significant variations with experimental results. In order to account for the significant anisotropy in the mixing vessel, a multiple-scale model proposed by Hanjalic et al. (1980) is used in this work.

The model developed herein, which enables the flow patterns to be calculated for a baffled tank agitated by a Rushton-type turbine impeller, is employed to calculate the profiles of the mass flow rate, mean velocity, and large-scale turbulence. The flow patterns are modeled by solving the transport equations for vorticity, stream function, and tangential momentum. The Reynolds stresses are modeled by means of the turbulent viscosity expressed by use of the second Prandtl hypothesis (Eq. 7). The scale of large energy-containing vortices in Eq. 7 is assumed constant within the whole volume of the tank, and the kinetic energy belonging to these vortices is computed from its transport equation.

Boundary conditions used in this work for the impeller region are based on earlier work by Placek and Tavlarides (1985), on the symmetry of the flow, and on the wall jet boundary layer flow.

Further, the original algorithm of Gosman et al. (1969) is corrected to account for the effect of false diffusion caused by the asymmetric finite-difference approximations, and an improved substitution formula is employed for modeling the diffusion terms.

The results of computations are in reasonable agreement with experimental measurements of the mean velocity at the tank wall. The computed profiles of kinetic energy of large vortices k_p and the effective viscosity μ_{eff} indicate that there is intensive convective transport of large-scale turbulence from the impeller region to the tank wall and along it. As the values of k and μ_{eff} do not vary signficantly in the remaining volume of the tank, the assumption of the local equilibrium between the production and consumption of turbulent energy in these regions is reasonable. The computed results show good agreement with reported circulation time correlations in the Rushton turbine-agitated vessel.

The general formulation of the boundary conditions for the impeller discharge flow used in this work allows the employment of the model for scale-up so long as a highly turbulent flow exists within the tank.

Literature Review

The flow patterns in mechanically agitated tanks have been extensively investigated experimentally during the last twenty years. The mean velocity profiles measured by Nagata et al. (1959) and Nagase et al. (1974) in baffled tanks equipped with paddle impellers indicated that mean velocities within the tank volume can be normalized by the impeller tip velocity. Nielsen (1958), DeSouza and Pike (1972), and Fořt et al. (1979a) showed that velocities in the discharge flow from the turbine impeller can be normalized by impeller diameter and rotational speed. The same parameters were used by Fořt et al. (1979b) for normalization of the wall jet flow along the tank wall.

Mujumdar et al. (1970), Rao and Brodkey (1972), Gunkel and Weber (1975), van't Riet et al. (1976), and Fořt et al. (1979a) found that the velocity fluctuations in the impeller discharge flow are strongly anisotropic, with a periodic component generated by the passage of the trailing vortices behind the impeller blades. The one-dimensional energy spectra of turbulence registered in this region cannot yield correct values of turbulence parameters due to the anisotropy of the flow. Simplified calculations based on the assumption of isotropic turbulence in the impeller discharge flow presented by Cutter (1966), Mujumdar et al. (1970), and Komasawa et al. (1974), predict excessive values of dissipation rates of turbulence (about 20 times greater than the mean bulk value) and lower values of the macroscale of velocity fluctuations (equal approximately to half the blade width). The results of Okamoto et al. (1981), which were corrected by anisotropic turbulence, indicate that the value of the dissipation rate of turbulence within this region is about six times greater than the bulk mean value, and that about 70% of the turbulent energy is dissipated in the bulk of the tank. The same conclusions resulted from the data of Günkel and Weber (1975), who analyzed the turbulence spectra registered throughout the tank. From their results it also follows that the value of the macroscale of turbulence within the whole tank remains nearly uniform, and approximately equal to the impeller blade width. Similar values of dissipation rate and macroscale of turbulence were obtained by Placek and Tavlarides (1985), who employed the concept of the trailing vortex introduced by van't Riet (1975), for modeling the mean and fluctuating velocities in the impeller discharge flow.

The mathematical modeling of the flow in an agitated tank is restricted by complicated flow patterns. The analytical models tend to oversimplify the complexity of the flow, and therefore can predict only the mean velocity profiles. DeSouza and Pike (1972) and Drbohlav et al. (1978) published analytical models of the turbine impeller discharge flow based on the concept of the tangential jet introduced by Nielsen (1958). Yamamoto and Nagata (1962) derived equations describing the profiles of tangential velocity component and static pressure in an unbaffled tank, and a similar model was presented by Platzer and Noll (1981). DeSouza and Pike (1972) combined the model of the tangential jet with the numerical solution of the continuity equation in the remaining volume of the tank. A similar approach was used by Ambegaonkar et al. (1977), who corrected the calculated velocity profiles using published data. They also evaluated the local values of fluctuation velocity assuming a constant value of the relative intensity of turbulence throughout the tank. A similar, though more elaborate, model was published by Fořt et al. (1982). Van't Riet and Smith (1975) related the high values of turbulence intensities to the pair of trailing vortices behind each impeller blade. Their results and the data of van't Riet (1975) indicated that:

1. Trailing vortices originate behind the inner edge of the blade (l in Figure 1), and later move outward along the horizontal blade edge.

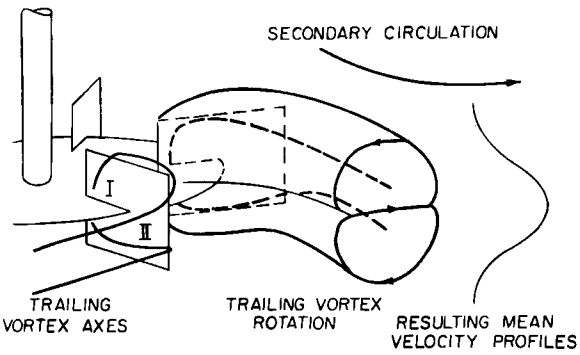

Figure 1. Trailing vortices behind Rushton-type turbine impeller and resulting mean velocity profile.
Notice opposite rotation of trailing vortices at contact with secondary flow.

2. The new positions of the vortex axes are established in vertical distances approximately equal to half the distance between the horizontal blade edge and the impeller disk plane, prior to reaching the outer blade edge (*II* in Figure 1).
3. The vortices rotate in countercurrent directions.
4. The position of trailing vortices does not change for $1.5 \times 10^4 \leq Re_M \leq 9 \times 10^4$.
5. The pressure changes are significant.

The trailing vortex concept was used by Placek and Tavlarides (1985) to create a new impeller discharge outflow model based on the actual existing mechanism. They obtained reasonable agreement with the data of Günkel and Weber (1975) by combining the vortex motion with uniform impeller outflow, and then averaging the instantaneous velocity with respect to the trailing vortex passage along a fixed point. The analysis of Placek and Tavlarides also indicates that the geometric similarity of the trailing vortices exists for the impeller size $D < T/2$ and that trailing vortices exist up to the radial distance $r \leq 0.7D$.

Utilizing the stream function-vorticity transformation, Thiele (1972) obtained the first numerical solution of the Navier-Stokes equation for an unbaffled tank. Given the symmetric difference approximations used for the convective terms, the stability of the algorithm was guaranteed only at low Reynolds mixing numbers, $Re_M \leq 20$. Placek et al. (1978) presented the first numerical solution for the fully turbulent flow. Assuming isotropic turbulence in the whole tank, they modeled the effect of turbulence using effective viscosity. Simple k-ϵ balance equations proposed by Launder and Spalding (1972) were employed. Placek et al. (1978) found reasonable agreement of calculated mean velocity profiles with the experimental results. However, calculated profiles of turbulent parameters were not compared with experimental data. Platzer (1981) published a nearly identical solution. However, this model employed simplified boundary conditions at the tank wall that were inappropriate with respect to the grid spacing utilized. A similar model was presented by Harvey and Greaves (1982). Their algorithm lacked a reliable boundary condition for turbulence parameters in the impeller region, where only gradients of mean velocity components determined the levels of turbulence. Placek (1978) also presented the numerical solution for the flow of a pseudoplastic fluid in an agitated tank.

Günkel and Weber (1975) found near-isotropic turbulence within the recirculation region. Assumed isotropic turbulence enabled them to obtain reliable values of turbulence macroscale Λ, which were found to be almost uniform throughout the whole region. With increasing specific power input, Placek and Tavlarides (1985) found values of Λ within the vessel approaching the diameter of the trailing vortices. Their analysis of the data published by Günkel and Weber yielded macroscale values within the interval $0.007D \leq \Lambda \leq 0.16D$, with most values of Λ greater than $0.1D$. Günkel and Weber also did not find significant differences in Λ for two different blade widths, $h = 0.2D$ and $h = 0.4D$. However, factors to determine the value of Λ within the tank remain unknown. There is also a great deal of evidence (Launder and Spalding, 1972) that in the developed free turbulent flows the motion of the large energy-containing eddies is independent of the Reynolds number, and that their size varies remarkably little within the flow field.

Furthermore, Günkel and Weber reported nearly uniform values of turbulence intensities throughout the recirculation region, having a variation about the space average of the order of 15%. Their results are indirectly confirmed by small differences in local mass transfer rates (approximately 20%) as reported by LeLan and Angelino (1974). They also found the turbulence intensity not to be related directly to the tank-impeller geometry, but indirectly through the power per unit mass and the specific impeller power input. The mean and RMS velocities within the vessel are proportional to the impeller circumferential velocity, and consequently, to the impeller rotational speed N. Assuming that the local production rate of turbulence is proportional to the product of turbulent viscosity and squared mean velocity gradients, the hypothesis of local equilibrium of turbulence leads to intensity of turbulence proportional to N^2. In spite of an unclear mechanism of turbulence transfer, the presence of trailing vortices in the impeller discharge flow does not support the assumption of the local equilibrium between the production and dissipation of turbulence. Thus, the convective transport of turbulence must be considered.

The presence of baffles results in axial asymmetry of the flow. Results of Nagata (1975) and Platzer (1981) show a steep decrease of the tangential component of mean velocity $\bar{v}_\theta$ in the impeller discharge flow, and an almost constant value of $\bar{v}_\theta$ in the recirculation region. The data of Nagata locate the axial asymmetry to the vicinity of baffles where the recirculation vortices occur. Recirculation flow behind the baffles was also observed by Placek et al. (1978). Fořt et al. (1980) found low turbulence in the impeller flow region with relative intensities not exceeding 5%.

Each of the cited models of turbulent flow in an agitated vessel displays discrepancies with experimental data. The most severe differences appear in the parameters these models are intended to predict, i.e., in profiles of k and ϵ. Using the simple k-ϵ model results in a steep decrease of turbulence with increasing distance from the impeller region. Placek (1980) found three orders of magnitude difference in profiles of ϵ. Similar profiles for k and ϵ published by Platzer (1981) display differences of magnitude four and five, respectively. The results of Harvey and Greaves (1982) show only one order of magnitude difference in profiles of k, and two orders of magnitude difference in profiles of ϵ. Considering the employed boundary condition for impeller turbulence, their results cannot be considered surprising. Published differences between predicted maximum and minimum values of k and ϵ found in the recirculation region (i.e., outside

the impeller discharge flow) are smaller. Placek's (1980) profiles of k and ϵ show differences of magnitude one and two, respectively. Data of Platzer (1981) display higher differences in k and ϵ profiles. Günkel and Weber (1975) found nearly uniform values of turbulence intensity throughout the recirculation region, having a variation about the space average of the order of 15%. Further, Okamoto et al. (1981) evaluated the local values of dissipation rate from the energy spectra. Their data show small differences throughout the whole tank, with the ratio of maximum and minimum values approximately equal to 20. A similar variation in ϵ profiles was found by Nagata (1975). Consequently, the experimental results indicate more homogeneous turbulence than is predicted by mathematical models.

The crucial check of a mathematical models' reliability is the energy balance. Mechanical energy transmitted to the fluid by the impeller is ultimately dissipated to heat, mostly through the cascade of turbulent vortices. The mass integrated dissipation rate of turbulence over the entire tank therefore must correspond to the value predicted for the impeller power input correlation. Placek's (1980) computations of the total energy dissipated by turbulence yielded only 12.6% for $T/D = 3$ and 30.8% for $T/D = 4$. Harvey and Greaves (1982) published the value 15.6% for $T/D = 2$. Platzer (1981) did not report any energy balance.

The system investigated in this study consists of a cylindrical, flat-bottomed vessel fitted with four vertical baffles equally spaced around the perimeter. The shaft of a Rushton-type turbine impeller is concentric with the axis of the vessel. In order to obtain a flow pattern comprised of two recirculation loops, the following conditions must be satisfied:

1. The impeller must not be placed too close to the bottom nor too close to the fluid level.
2. The mixing must be fully turbulent
3. The impeller rotational speed N must be low enough to prevent flooding of the impeller by either caviation or by suction of air from the central vortex.

Then the flow field can be divided into two main regions: the impeller discharge flow, and the recirculation flow in the remaining volume of the vessel. Only a portion of the recirculation fluid passes through the impeller zone, since the secondary recirculation is caused by the momentum transfered to the fluid in the impeller discharge flow region.

It is useful to introduce the following convention in terminology. Turbulent flow is defined as "an irregular condition of flow in which various quantities show a random variation with time and space coordinates, so that statistically distinct average values can be discerned" (Hinze, 1975). Therefore, the trailing vortices behind the impeller blades, the vortices behind the baffles, and other regular motions would not be considered as turbulence. Such phenomena have been referred to as pseudoturbulence by van't Riet et al. (1976) and more recently as velocity fluctuations by Placek and Tavlarides (1985). The approach is distinct from recent studies of coherent structures (Cantwell, 1981; Hussain, 1983) in that we are lumping the regular and turbulent motions together in the description of the turbulent energy. In the agitated vessel, however, the regular motions and turbulence are so closely connected that to continue a permanent distinction between them would only complicate the description of the problem. Consequently, all velocity fluctuations discussed herein are considered as turbulence, and one needs only to keep in mind the distinction between regular and random motions.

Physical Model

The semiempirical nature of the available turbulence models requires careful consideration of the actual physical system when selecting a model. The modeled equations for k and ϵ have been extensively applied to a large number of engineering applications. The relative simplicity and success of these models for a large number of flows has been reviewed by Rodi (1980) and Bradshaw et al. (1981). As pointed out earlier, the classic k-ϵ model does not adequately describe the energy distribution throughout a mixing vessel.

Large-scale turbulence

Figure 2 sketches energy transfer in an agitated vessel. The mechanical energy of the rotating impeller is transmitted both directly to the recirculation of the fluid, and to the large convective vortices. Since the motion of large vortices is not stable, it gives rise to smaller vortices. This process continues toward smaller and smaller eddies until the viscous forces become important, and the mechanical energy is finally transformed to heat in the smallest eddies. No measurements of direct dissipation in agitated vessels have been reported. The other portion of the energy of the recirculation flow is transferred to the energy of the large vortices by the mean velocity gradients. Modeling the anisotropic turbulence would demand simultaneous solution of transport equations for all turbulence correlations. The requirement of balancing turbulence correlations separately is not necessary if the turbulence is isotropic. However, the previous analysis of the impeller discharge flow indicates that turbulence can be considered isotropic in the remaining tank volume. It is assumed here that an isotropic turbulence model is sufficient if it includes the proper correction for the effect of trailing vortices on the secondary recirculation flow. Such correction would express a lower increase of radial momentum near the impeller region, compared to the value predicted by the high value of turbulent viscosity ν_t. Since most of the turbulence energy is contained in large vortices, the turbulent viscosity ν_t and length scale are related to their properties, and are characterized by the macroscale Λ. Furthermore, the macroscale energy balance must consider the transfer rate of turbulent energy to the smaller eddies. A two-dimensional model is suggested such that in the recirculation region, the large vortices are generated by mean velocity gradients in the r-z plane. Consequently, the large vortices are similarly oriented in the r-z plane. The tangential momentum of the impeller discharge flow is transformed by the action of the baffles either into axial momentum or into the large vortices behind the baffles. These vortices are carried by the recirculation flow upward along the wall to the center of the tank. The interaction of the impeller discharge flow with the recirculation flow gives rise to large vortices in the r-z plane.

Small-scale turbulence

The commonly adopted route to model the transport equation for turbulence energy is to assume that the transfer rate of tur-

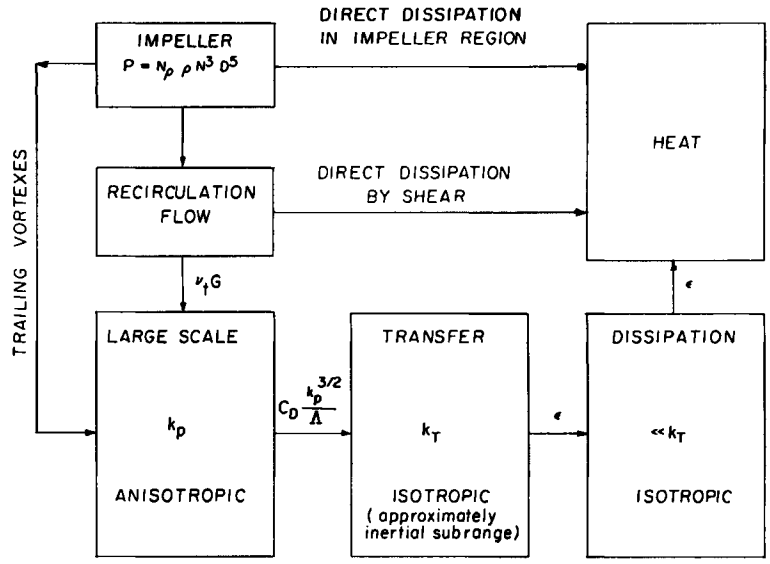

Figure 2. Model of dissipation of mechanical energy in an agitated vessel.

bulence energy to the smaller eddies is the dissipation rate of turbulence ϵ, and solve the approximate transport equation for ϵ. Referring to Figure 2, such an approach implicitly assumes the spectral equilibrium of turbulence. However, the recorded energy spectra refute spectral equilibrium of turbulence in the impeller discharge region. Further, the large vortices generated by baffles are carried from the place of their origin by the recirculation flow. Their presence can also cause the spectral nonequilibrium of turbulence. The velocity gradients in the recirculation region (far from the vessel wall) are smaller, and therefore the production rate of large vortices in this region is also smaller. Due to their age, the turbulence energy of the carried vortices is meanwhile transferred to the smaller eddies. Consequently, in some parts of the recirculation region the energy-containing vortices can also be associated with length scales smaller than Λ. These indications suggest modeling of the Reynolds stresses as a function of turbulent motions that belong to the different scales.

The simplest multiple-scale model of turbulence is created by dividing the energy spectrum of turbulence into the three parts, namely, large-scale vortices, intermediate or transfer eddies, and dissipation eddies. Given the negligible energy content of the latter, the multiple-scale model of turbulence consists only of separate balance equations of turbulent energies belonging to the large-scale vortices and to the transfer eddies, respectively. The kinetic energy of the latter is produced at a rate equal to the energy transfer rate from large-scale vortices. It is then lost by transfer to the dissipation eddies, as characterized by the dissipation rate. The transfer eddies can be associated with the inertial subrange in the turbulence energy spectra. The balance equations for the two-scale turbulence model can then be stated as:

$$\frac{Dk_P}{Dt} = \frac{\partial}{\partial x_i}\left(\frac{\nu_t}{Sc_k}\frac{\partial k_P}{\partial x_i}\right) + \nu_t G - C_D\frac{k_P^{3/2}}{\Lambda} \tag{1}$$

$$\frac{Dk_T}{Dt} = \frac{\partial}{\partial x_i}\left(\frac{\nu_t}{Sc_k}\frac{\partial k_T}{\partial x_i}\right) + C_D\frac{k_P^{3/2}}{\Lambda} - \epsilon \tag{2}$$

where

$$G = \left(\frac{\partial \bar{v}_r}{\partial z} + \frac{\partial \bar{v}_z}{\partial r}\right)^2 + \left(\frac{\partial \bar{v}_\theta}{\partial r} - \frac{\bar{v}_\theta}{r}\right)^2 + \left(\frac{\partial \bar{v}_\theta}{\partial z}\right)^2 \tag{3}$$

$$\Lambda = C_\Lambda D \tag{4}$$

Here k_P and k_T are the kinetic energies of turbulence belonging to the large-scale vortices and to the transfer eddies, respectively. The value of the empirical constant C_Λ results from analysis of the published experimental data. The commonly used balance equation for the dissipation rate of turbulence ϵ is presented by Launder and Spalding (1972) as:

$$\frac{D\epsilon}{Dt} = \frac{\partial}{\partial x_i}\left(\frac{\nu_t}{Sc_\epsilon}\frac{\partial \epsilon}{\partial x_i}\right) + C_2\nu_t G\frac{\epsilon}{k} - C_\epsilon\frac{\epsilon^2}{k} \tag{5}$$

Here Sc_ϵ is the Schmidt number for the turbulent diffusion of ϵ. C_2 and C_ϵ are identified as empirical constants. The production term in Eq. 5 is based upon the mean velocity gradient. Consequently, the production rate of ϵ is bound to the time scale of the mean flow. Considering different transfer rates of turbulence energy at different parts of the energy spectra, the production term in Eq. 5 should be based on the energy transfer rate of the large-scale vortices, as indicated by the analysis of Hanjalic et al. (1980). Thus, the product of $\nu_t G\epsilon$ can be replaced by the squared energy transfer rate from large vortices, $(C_D k^{3/2}/\Lambda)^2$. Further, the dissipation rate ϵ should be related to the energy transferred by its own action, rather than to the overall kinetic energy of turbulence. Incorporating these assumptions, the transport equation can be restated as:

$$\frac{D\epsilon}{Dt} = \frac{\delta}{\delta x_i}\left(\frac{\nu_t}{Sc_\epsilon}\frac{\delta \epsilon}{\delta x_i}\right) + C_P\frac{k_P^3}{\Lambda^2 k_T} - C_\epsilon\frac{\epsilon^2}{k_T} \tag{6}$$

Here C_P is another empirical constant.

Turbulent viscosity

The turbulent viscosity ν_t should be characterized by both k and ϵ. A form similar to that proposed by Hanjalic et al. is used in the model:

$$\nu_t = C_\mu \frac{k_P + k_T}{\sqrt{k_P}} \Lambda \tag{7}$$

The suggested expression for the turbulent viscosity ν_t ensures that for $k_P > k_T$, the value of ν_t approaches the limiting value given by $\nu_t = C_\mu \ell \sqrt{k}$ where C_μ is an empirical constant. Further, the value of ν_t is not equal to zero if it is given that the energy of large vortices has already transferred into the smaller eddies, but has not yet dissipated.

The values of constants assigned to the turbulence model are based on the data of Danon et al. (1977) and Hanjalic et al. (1980):

$$C_D = 1.0 \qquad C_\epsilon = 1.15$$
$$C_P = 1.08 \qquad Sc_k = 1.0$$
$$C_\Lambda = 0.14 \qquad Sc_\epsilon = 1.0$$
$$C_\mu = 0.078$$

Discussion

Unlike the commonly used k-ϵ model of turbulence, the proposed model offers a capability to model the dynamic response of turbulence to the local changes of turbulence production in an agitated vessel. Since, in this particular case, the turbulence production is not necessarily related to the mean velocity gradients, it was necessary to introduce an alternative balance equation for the dissipation rate of turbulence ϵ. The validity of Eq. 5 in modeling the spectral nonequilibrium flows is somewhat dubious since it assumes that the local production rate of ϵ is dependent on local mean strain. In fact, however, the mean strain affects the dissipation rate ϵ only indirectly via the vortex cascade transfer mechanism. Consequently, Eq. 5 is more or less a balance equation for the energy transfer rate associated with the large-scale turbulence. As such, it can be considered as a balance of the dissipation rate ϵ only for spectral equilibrium flows. Alternatively, when Eq. 6 is employed, a sudden drop of shear stress results only in decreased production of large-scale turbulence, while simultaneously the value of ϵ decreases gradually as k_P is transferred to k_T. The energy transfer rate from the large-scale vortices therefore acts as a precursor of changes in the dissipation rate of turbulence ϵ.

Further, the production of the large-scale turbulence, not associated with mean velocity gradients (i.e., the effect of trailing vortices), can easily be modeled by the introduction of an additional production term in Eq. 1. Such a change automatically causes a proper increase of ϵ due to the k_P production term in Eq. 6.

A basic point of the model is the division between the large-scale vortices and the transfer eddies region. As the partition moves toward very small vortex scales, only a small portion of the total energy would be contained in k_T, and the time for energy to cross the transfer region would be negligible. In such a case both the energy transfer rates are approximately equal, and the two-scale model reduces to the commonly used k-ϵ model. On the other hand, if the partition moved toward very large vortices, it would result in an unsatisfied assumption of local isotropy. Consequently, this condition results in incorrect values of the dissipation rate ϵ. Too low a value of partition frequency could also violate the assumption of zero production of k_T by strain. Hanjalic et al. (1980) recommended the presented values of C_P and C_ϵ for the approximate modeling of the inertial subrange turbulence. It is not clear whether the value of k_T is identical to the energy of inertial subrange eddies. Since a small change in partition can significantly change the value of k_T, we suggest using the calculations of other properties of vortices belonging to the universal equilibrium range upon the value of ϵ rather than upon the turbulent energy of the subrange eddies k_T.

It is not completely clear where the division between the large-scale turbulence and the recirculation macroflow should be positioned. The size of the reverse recirculation loop, at the intersection of the tank wall and fluid level, is comparable with the size of trailing vortices. Neither the reverse recirculation and/or the circular rotation of the fluid at the impeller axis, nor the core of the main recirculation loop are referred to as turbulence. The division used in this model was inspired mainly by the energy content of different vortices, and its flexibility should be kept in mind.

The assumption of isotropic or near-isotropic turbulence is strongly violated in the impeller discharge region. The value of the turbulence viscosity predicted by Eq. 7 for this region is untenably high, and a proper correction of the mean momentum transfer equations and/or boundary conditions must be employed. The guidelines for its quantification can be based on the model of Placek and Tavlarides (1985). To accomplish this, the stream function value (or the mean velocity profile) at the horizontal borders of the impeller discharge flow should be properly prescribed. Keeping the value of the stream function constant up to the distance where the trailing vortices exist satisfies the above requirement for correction.

Mathematical Model

Governing equations

The turbulent flow in a baffled tank equipped with a Rushton-type turbine impeller is essentially three-dimensional, with steep gradients of velocity and pressure. As there is a lack of reliable data to describe the pressure changes around the impeller (Drbohlav et al., 1978; van't Riet and Smith, 1975), it is desirable to eliminate the pressure from the flow equations. This is done by transformation of radial and axial velocity components into the new variables, stream function $\bar{\Psi}$ and vorticity $\bar{\omega}$,

$$\bar{\Psi} = \int \rho r \bar{v}_z \, dr = -\int \rho r \bar{v}_r \, dz$$
$$\bar{\omega} = \frac{\partial \bar{v}_r}{\partial z} - \frac{\partial \bar{v}_z}{\partial r} \tag{8}$$

The tangential momentum is balanced separately. The $\bar{\Psi}$-$\bar{\omega}$ transformation is conditioned by the assumption of axial symmetry of flow. The assumption of axial symmetry is mainly violated near the tank wall (Nagata, 1975; Nagata et al., 1958, 1959; DeSouza and Pike, 1972), and a substantial error in the overall flow pattern can be introduced. Consequently, the necessity for a tangential velocity correction in the tank wall boundary condition is indicated.

The Reynolds stresses are modeled by means of the turbulent viscosity based on the three-equation model of turbulence presented earlier. The effective viscosity ν_{eff} is the sum of the turbulent viscosity ν_t and the molecular viscosity ν. The contribution of the molecular viscosity to the effective viscosity is negligible for most cases and can be ignored. This definition, however, prevents potential numerical instabilities, which could be caused by a zero value of the effective viscosity at the beginning of the computations.

A detailed description of the transport equation for a general transport variable ϕ and associated derivatives is given by Gosman et al. (1969). Assuming axial symmetry, steady flow, and incompressible fluid, the transport equation is:

$$A\left[\frac{\partial}{\partial z}\left(\phi\frac{\partial\overline{\Psi}}{\partial r}\right)-\frac{\partial}{\partial r}\left(\phi\frac{\partial\overline{\Psi}}{\partial z}\right)\right] - \frac{\partial}{\partial z}\left[Br\frac{\partial(C\phi)}{\partial z}\right]-\frac{\partial}{\partial r}\left[Br\frac{\partial(C\phi)}{\partial r}\right]-rS=0. \quad (9)$$

Here ϕ represents a general balanced variable such as $\overline{\Psi}$, $\overline{\omega}/r$, $\overline{v}_\theta r$, k_P, k_T, and ϵ. The expressions for the coefficients A, B, C, and S are listed in Table 1.

Boundary conditions

The system modeled consists of a baffled tank equipped with a Rushton-type turbine impeller, and the balanced volume is the region between the impeller disk plane and the fluid level, Figure 3. The origin of the cylindrical coordinates is located in the intersection of the tank axis and the impeller disk plane. The boundary conditions necessary for solution of Eq. 9 are summarized in Figure 4. The numerical solution thereby requires the assumptions of:

1. No slip at the wall from the wall jet model
2. Symmetry planes at the free surface and at the impeller disk plane
3. Axial symmetry at $r = 0$.

Also, the implicit numerical model for the impeller discharge flow described in Part I of this series (Placek and Tavlarides, 1985) provides a necessary boundary condition for the numerical solution of the flow in the vessel. This analysis models the impeller discharge flow to consider:

1. Spectral nonequilibrium in the region
2. Anisotropy in the impeller region

Table 1. Coefficients in Eq. 2.

ϕ	A	B	C	S
$\overline{\Psi}$	0	$\frac{1}{\rho r^2}$	1	$\frac{\overline{\omega}}{r}$
$\frac{\overline{\omega}}{r}$	r	r^2	μ_{eff}	$\frac{\partial}{\partial z}(\rho\overline{v}_\theta^2)$
$\overline{v}_\theta r$	1	$\mu_{eff}r^2$	$\frac{1}{r^2}$	0
k_p	1	$\frac{\mu_t}{Sc_k}$	1	$\mu_t G - C_D\rho\frac{k_P^{3/2}}{\Lambda}$
k_T	1	$\frac{\mu_t}{Sc_k}$	1	$C_D\rho\frac{k_P^{3/2}}{\Lambda}-\epsilon$
ϵ	1	$\frac{\mu_t}{Sc_\epsilon}$	1	$C_P\frac{k_P^3}{\Lambda^2 k_T}-C_\epsilon\rho\frac{\epsilon^2}{k_T}$

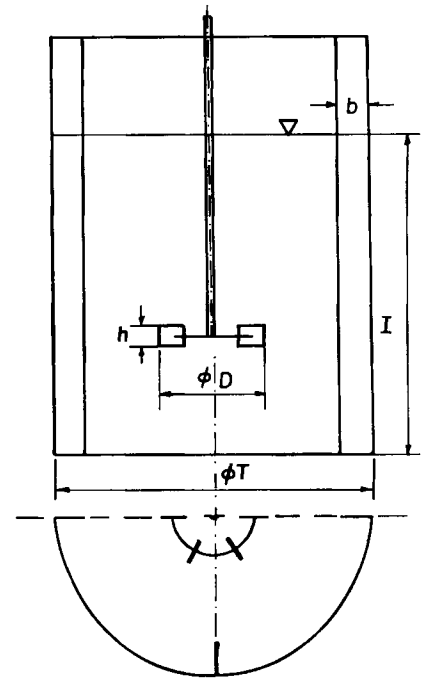

Figure 3. Baffled tank equipped with a Rushton-type turbine impeller.

3. Insignificant turbulence production by mean shear
4. Significant turbulence production by large-scale anisotropic vortices.

Impeller Region. The boundary conditions for the discharge flow from a Rushton-type turbine impeller established by Placek and Tavlarides (1985) are used. The values of stream function, vorticity, tangential momentum, and kinetic energy of large-scale vortices are evaluated for the row of grid nodes at the

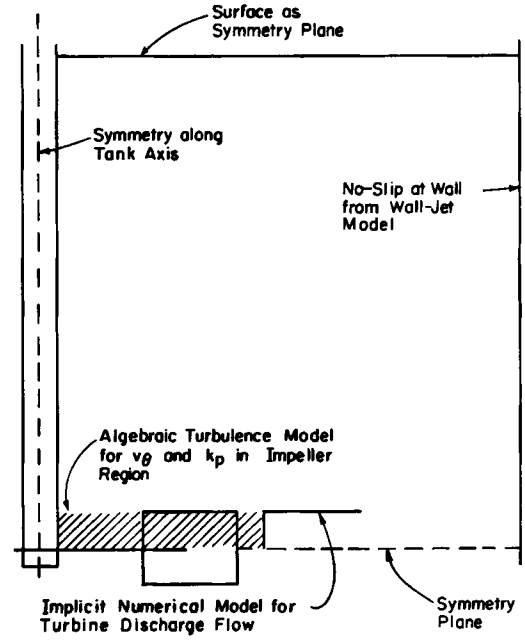

Figure 4. Boundary conditions imposed by vessel geometry.

radial distance $r = 1.08R$, from the impeller disk plane up to the impeller blade edge.

As indicated earlier, the untenably high value of turbulent viscosity predicted by the isotropic turbulence model would result in unrealistically high secondary recirculation. The action of trailing vortices, however, significantly decreases mean momentum transfer from the impeller region. In order to preserve the high values of k_P in the impeller region, and to respect the low mean momentum transfer to the secondary recirculation flow, the value of the stream function is kept constant. This condition is applied at the axial coordinate equal to the impeller blade edge, and within the interval of radial coordinates where the trailing vortices exist:

$$\begin{aligned} \bar{\Psi}(r) &= \bar{\Psi}(1.08R) && 1.08R \le r \le 1.4R \\ \bar{\omega}(r) &= \bar{\omega}(1.08R)\frac{1.08R}{r} && z = b/2 \end{aligned} \tag{10}$$

A boundary condition thus established declares mass flow through the horizontal boundaries of the impeller discharge flow equal to zero. From the continuity equation, it then follows that $\bar{v}_r$ is proportional to $1/r$. This dependency was confirmed by Cutter (1966) and by Mujumdar et al. (1970). The boundary condition for $\bar{\omega}$ follows from the continuity equation and from the assumed similarity of velocity profiles.

The values of k_P within the impeller region ($0 \le r \le R$) are set equal to those at the impeller outflow, and the tangential component of velocity is prescribed as the constant angular velocity equal to the impeller outflow value at the same axial coordinate:

$$\begin{aligned} \bar{v}_\theta(r, z) &= \bar{v}_\theta(R, z)\frac{r}{R} && 0 \le r \le 1.08R \\ k_P(r, z) &= k_P(1.08R, z) && 0 \le z \le 0.5h \end{aligned} \tag{11}$$

It is not necessary to specify the values of k_T and ϵ, since they are computed in the entire impeller region from their transport equations.

Impeller Disk Plane. The boundary conditions at the impeller disk plane are based on the horizontal symmetry of the flow, which can be declared as zero axial derivatives of the balanced variables except for vorticity, which is set equal to zero. Placek and Tavlarides (1985) showed that the trailing vortices exist up to the radial distance $r = 1.4R$. In order to express the high intensity of turbulence in the impeller discharge flow, the kinetic energy of large vortices k_P is balanced only for $r > 1.4R$, with zero shear stress at the impeller disk plane assumed. For smaller values of r the value predicted by the impeller boundary condition is used. The values of vorticity and stream function are set equal to zero:

$$\begin{aligned} k_P(r) &= k_P(1.08R) && 0 \le r \le 1.4R \\ \bar{\Psi}(r) &= 0 && z = 0 \\ \bar{\omega}(r) &= 0 \end{aligned} \tag{12}$$

Tank Wall. Fořt et al. (1979b) showed that the flow at the tank wall displays the features of a wall jet. The wall jet boundary layer concept is used for declaring the boundary condition at the whole wall, including the impingement region at the intercept of the impeller disk plane with the wall. The analysis of Ljuboja and Rodi (1980) indicates that in a wall jet boundary layer the logarithmic velocity profile holds for much smaller distances from the wall, since the piston velocity profile outside the boundary layer does not exist. The limit $y^+ \le 50$ is recommended. Here y^+ is a dimensionless wall distance $y^+ = u_* y/\nu$, $u_* = (\tau_w/\rho)^{1/2}$ is the friction velocity, and τ_w is the wall shear stress. Considering the buffer and laminar sublayers close to the wall, Ljuboja and Rodi proposed the following set of equations:

$$\begin{aligned} \bar{v}_z/u_* &= y^+ && 0 \le y^+ \le 5 \\ \bar{v}_z/u_* &= 5 \ln y^+ - 3.05 && 5 < y^+ \le 20 \\ \bar{v}_z/u_* &= 2.3 \ln y^+ + 5.05 && 20 < y^+ \le 50 \end{aligned} \tag{13}$$

The value of the coefficient 2.3 is close to the reciprocal value of the von Kármán constant κ. Substitution into Eq. 8 and integration between the near-wall grid node with index m and the wall grid node with index w yields:

$$\begin{aligned} \bar{\Psi}_m - \bar{\Psi}_w &= \mu[0.5 r_w y^+ - 0.33(r_w - r_m)y^+] && 0 \le y^+ \le 5 \\ \bar{\Psi}_m - \bar{\Psi}_w &= \mu\{[(5 \ln y^+ - 8.05)y^+ + 12.5]r_w \\ &\quad - [(2.5 \ln y^+ - 2.78)y^+ \\ &\quad - 31.2/y^+ + 8.33](r_w - r_m)\} && 5 < y^+ \le 20 \\ \bar{\Psi}_m - \bar{\Psi}_w &= \mu\{[(2.3 \ln y^+ + 2.75)y^+ - 41.7]r_w \\ &\quad - [(1.12 \ln y^+ + 1.38)y^+ \\ &\quad - 1{,}928/y^+ + 93.1](r_w - r_m)\} \\ &\quad 20 < y^+ \le 50 \end{aligned} \tag{14}$$

The value of y^+ is found numerically employing the Newton-Raphson iterative procedure. The known value of y^+ enables one to express the shear velocity u_* and the vorticity $\bar{\omega}$,

$$\begin{aligned} \bar{\omega} &= \frac{u_*^2}{\nu} && 0 \le y^+ \le 5 \\ \bar{\omega} &= \frac{5u_*^2}{\nu y^+} && 5 < y^+ \le 20 \\ \bar{\omega} &= \frac{2.3u_*^2}{\nu y^+} && 20 < y^+ \le 50 \end{aligned} \tag{15}$$

The distance of the near-wall grid line from the wall has to be adjusted to fall within the interval $20 < y^+ \le 50$, preferably close to the upper limit. Launder and Spalding (1974) showed that outside the laminar sublayer (i.e., in the region where the velocity profile obeys the logarithmic law of the wall) the turbulent shear stress can be assumed to be approximately equal to the wall shear stress ($\mu_t \partial \bar{v}_z/\partial r = \tau_w$), if the dissipation and the production of the kinetic energy of turbulence are in equilibrium [$\nu_t(\partial \bar{v}_z/\partial r)^2 = \epsilon$]. Considering turbulent viscosity ν_t in the boundary layer as $\nu_t = C_\mu k^2/\epsilon$, the boundary layer condition for k is

$$k_m = C_\mu^{-1/2} u_*^2 \tag{16}$$

and it also suggests that the value of k_m is related to small-scale turbulence rather than to the turbulent energy of large vortices. Nevertheless, the lack of other boundary conditions results in

using Eq. 16 for k_P and for k_T. Assuming that the rate of turbulence energy production is equal to $u_*^2(\partial\bar{v}_z/\partial r)$ and taking $\partial\bar{v}_z/\partial r$ from Eq. 14, there results the following boundary condition for turbulence parameters:

$$k_P = k_m$$
$$k_T = k_m \quad 20 < y^+ \leq 50$$
$$\epsilon = \frac{u_*^3}{\kappa(r_w - r_m)} \tag{17}$$

The effect of the tangential component of mean velocity at the wall is not considered either for the boundary condition for the vorticity, or for the turbulence variables.

The effect of baffles on the $\bar{v}_\theta$ profiles in the near-wall region is modeled by employing the experimentally determined velocity direction at the wall; see Figures 5 and 6. There appears to be a nearly uniform value of flow direction at the wall at almost all points. The average value of 20° between v_θ and v_z is used for the boundary condition as:

$$\bar{v}_\theta(r, z) = |\bar{v}(r, z)| \tan 20° \quad \begin{matrix} (T/2 - b) \leq r \leq T/2 \\ 0 \leq z \leq 0.62H \\ |\bar{v}_z| > |\bar{v}_r| \end{matrix} \tag{18}$$

The condition $|\bar{v}_z| > |\bar{v}_r|$ is used in order to prevent the steep decrease of $\bar{v}_\theta$ in the impinging region.

Escudier's (1966) analysis of the experimental data on the mixing length distribution near the wall indicates that except for

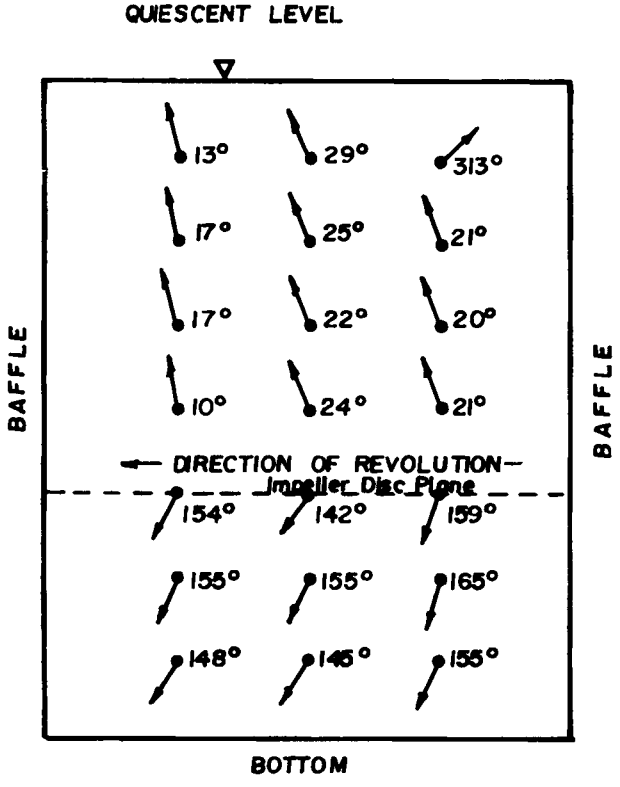

Figure 5. Flow directions at tank wall and standard deviations for $T/D = 3$, $N = 400$ min^{-1}.

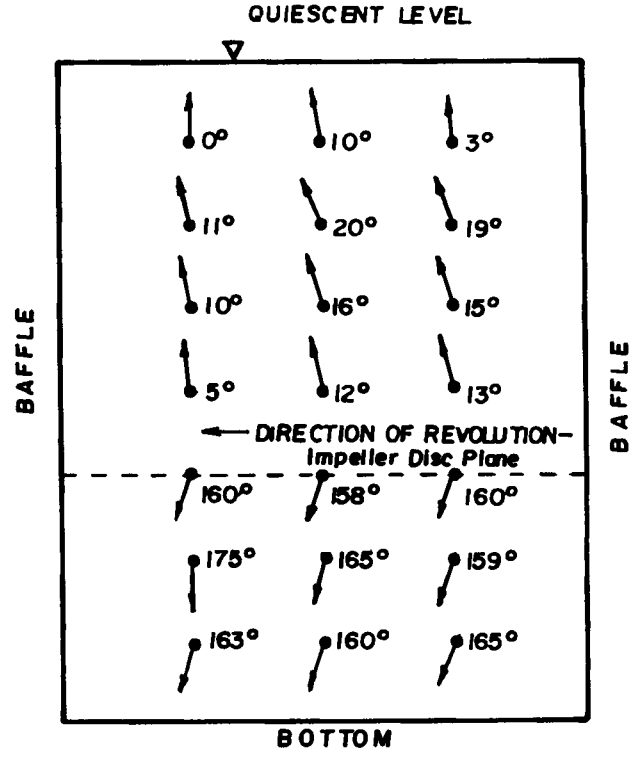

Figure 6. Flow directions at tank wall and standard deviations for $T/D = 4$, $N = 840$ min^{-1}.

the laminar and buffer sublayers, the mixing length increases linearly with distance from the wall. Assuming a similar distribution for the macroscale of turbulence, the value of Λ in the near-wall region is set equal either to the value given by the trailing vortex model or to the distance from the wall, whichever is smaller. On the other hand, Nagata et al. (1959) observed a form separation around the baffles resulting in the generation of large eddies. This effect is expressed in the region equal to the baffle width by increasing the value of Λ to $0.6b$, while the above-mentioned condition of the wall damping is still respected.

Integrating the Navier-Stokes equations through the boundary layer and applying the appropriate Ψ, ω transformation gives the boundary condition for $\bar{\omega}_w$:

$$\bar{\omega}_w = \frac{8(M^2 - 1)(M - 1)^2}{(M^2 - 1)(3 - M^2) - 4 \ln M} \frac{\bar{\Psi}_m - \bar{\Psi}_w}{\rho(r_w - r_m)r_w} + \frac{M^4 - 1 - 4M^2 \ln M}{M(M^2 - 1)(3 - M^2) - 4M \ln M} \bar{\omega}_m \tag{19}$$

where $M = r_w/r_m$. The value of the stream function at the wall is set equal to zero:

$$\Psi_w = 0 \tag{20}$$

Free Surface. The turbulence variables at the free surface are balanced in the same way as was employed for the impeller disk plane. The value of the stream function is set equal to zero. The boundary condition for vorticity follows from the assigned velocity profile, which yields zero axial derivative of $\bar{\omega}$ at the bounda-

ry. The zero axial derivative is also prescribed for the tangential velocity component.

$$\begin{aligned} &\overline{\Psi}(r) = 0 \\ &\frac{\partial \overline{\omega}(r)}{\partial z} = 0 \quad 0 \le r \le 0.5T \\ &\qquad\qquad z = 0.62\mathrm{H} \\ &\frac{\partial \overline{v}_\theta(r)}{\partial z} = 0 \end{aligned} \tag{21}$$

Impeller Shaft. The flow at the impeller axis is modeled as an axially symmetric jet, ignoring the presence of the impeller shaft. The tangential velocity component at the axis is set equal to zero and the turbulence variables are balanced assuming zero shear stress at the axis. The boundary condition for $\overline{\omega}/r$ is based on the parabolic profile near the axis, as proposed by Gosman et al. (1969).

$$\begin{aligned} &\overline{\Psi} = 0 \\ &\frac{\overline{\omega}}{r} = \frac{8}{\rho} \frac{(\overline{\Psi}/r^2)_2 - (\overline{\Psi}/r^2)_1}{r_1^2 - r_2^2} \quad r = 0 \\ &\overline{v}_\theta = 0 \end{aligned} \tag{22}$$

Here indexes 1 and 2 denote grid nodes once and twice removed from the tank axis, respectively.

Solution procedure

To solve the finite-difference counterparts of Eq. 9 the flow field is covered by a nonequidistant network refined at the wall and at both horizontal boundaries. Equation 9 is replaced at each point of the grid by a finite-difference equation that is recast as a successive-substitution formula. This system of equations, with the coefficients expressed in terms of the grid node values, is solved by the Gauss-Seidel point iterative procedure with upwind differencing employed as described in the Appendix, which is available as supplementary material.

The computational algorithm is an improved version of that published by Gosman et al. (1969). The original algorithm does not satisfy the conservation principle when the nonequidistant cylindrical coordinates and the balancing of the boundaries are employed. Further, arithmetic means of the interface diffusivities were originally used instead of the correct harmonic means. Appropriate corrections are made here, together with the reduction of the error caused by upwind difference approximations. The use of asymmetric difference approximations (which are necessary for the stability of the algorithm) results in smearing of the large gradients of the balanced variables. This effect can be formally expressed as an increased diffusion, and is designated as false diffusion. Wolfshtein's (1967) analysis of the impinging flow indicates that the largest errors caused by this phenomenon appear in the impingement region, where the streamlines are inclined to the grid lines. The correction suggested by Patankar (1980) is incorporated here.

Experimental

Experimental setup

Experiments were carried out in a cylindrical, flat-bottomed tank with diameter $T = 0.294$ m, having four baffles of width $b = 0.1T$ equally spaced around the perimeter, and equipped with a Rushton-type turbine impeller with a ratio of diameter to blade length to blade height of 20:5:4. The tank was filled with water up to a height $H = T$, and the impeller lower blade edge was positioned at a height $T/3$ above the bottom. Two sizes of impeller were used, $D = T/3$ and $D = T/4$. The Reynolds mixing numbers were $Re_M = 63{,}300$ for $D = T/3$ ($N = 400$ min^{-1}) and $Re_M = 72{,}800$ for $D = T/4$ ($N = 840$ min^{-1}).

Measurements of mean velocity

The sensor was a miniaturized three-hole Pitot tube made from hypodermic needles of 1 mm OD, with the two side openings tilted at an angle of approximately 45° in order to obtain maximum directional sensitivity. The directional sensitivity of the central opening was suppressed by reaming the tube to produce a 60° inside bevel. For details of the experimental setup see Fořt et al. (1979b). The directional sensitivities of the tilted and beveled openings were discussed by Folsom (1956). The recommended formula for the dynamic pressure head $\bar{p}_{\mathrm{dyn}}$ expressed as a function of the angle α between the velocity and the tube axis is

$$\bar{p}_{\mathrm{dyn}} = C_1 \rho \overline{v}^2 \cos (C_2 - \alpha)^2 \tag{23}$$

for the side openings, while the directional characteristics of the central opening fits Eq. 23 after a lag equal approximately to 30°. The Pitot tube was calibrated at three different velocities for ($-45° \le \alpha \le 45°$), and the parameters C_1 and C_2 were obtained as functions of velocity by means of a nonlinear regression.

Up to a distance of 30 mm, radial profiles of the mean velocity at the tank wall were measured for axial coordinates 37, 55.5, 74, 111, and 148 mm above the impeller disk plane, for each tangential position: $\theta = 22.5°$, $\theta = 45°$, and $\theta = 67.5°$ ($\theta = 0°$ at the baffle plate). The axes of the tubes were oriented in the same direction as the velocity at the wall, Figures 5 and 6, but with the openings facing against the flow. Further, the plane of the tube axes was in a plane normal to the tank wall. The pressure differences registered in the Pitot tube openings (using the quiescent fluid pressure as reference values) were first corrected graphically for the displacement of the openings. Then, these pressure differences were fed into the evaluation program based on the directional characteristics of the openings, Eq. 23, and on the pressure functions published by Fořt et al. (1969). The values of $\overline{v}$ and α were found numerically, employing the Newton-Raphson iterative procedure.

The accuracy of the mean velocity measurements depends on:

1. The accuracy of positioning the Pitot tube at the given location
2. The stability of the impeller rotational speed
3. The accuracy of the pressure head reading
4. The effect of the velocity gradient at the Pitot tube opening
5. The deceleration of the flow by the presence of the sensor
6. The interaction of the Pitot tube with the wall
7. The increase of the pressure head due to the turbulence.

Employing the relations published by Folsom (1956) and his own experimental data, Placek (1980) showed that the maximum relative error caused by points 1 through 4 and by point 6 does not exceed 10%; similar accuracy follows from the experi-

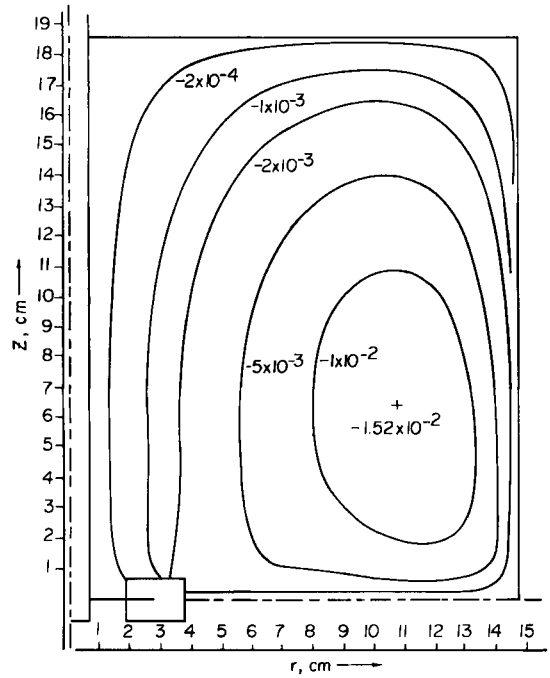

Figure 7. Calculated profiles of stream function $\bar{\Psi}$ in kg/s for $T/D = 4$, $N = 840$ min^{-1}.

ments of Kitaura et al. (1970). The effect of point 5 is supposed to be suppressed by the calibration. However, significant error is introduced by point 7. Substituting into Eq. 23 the velocity decomposed into the mean and fluctuating components, taking the time average, taking the derivative, and linearizing, yields the relation between the relative error of the mean velocity measurement Δv as a function of the relative intensity of turbulence δ,

$$\Delta v = \frac{\delta}{2(1 + \delta)^{3/2}} \tag{24}$$

Considering the representative value of δ given by Schwartzberg and Treybal (1968) as $\delta = 0.3$, Eq. 24 yields $\Delta v = 10.1\%$. A conservative estimate of the experimental accuracy of the mean velocity measured at the tank wall by means of the Pitot tube is, therefore, taken as 20%.

Results and Discussion

The reliability of the mathematical model was tested by comparison of the computed mean velocity profiles and stream functions (Figure 7) with experimentally determined values. The tank wall region was selected for several reasons. First, the measurements of velocity in the impeller discharge flow are inaccurate due to the high intensity and anisotropy of velocity fluctuations. Further, computed values of mean velocity close to the impeller would reflect the already confirmed boundary conditions for the impeller region rather than the numerical model

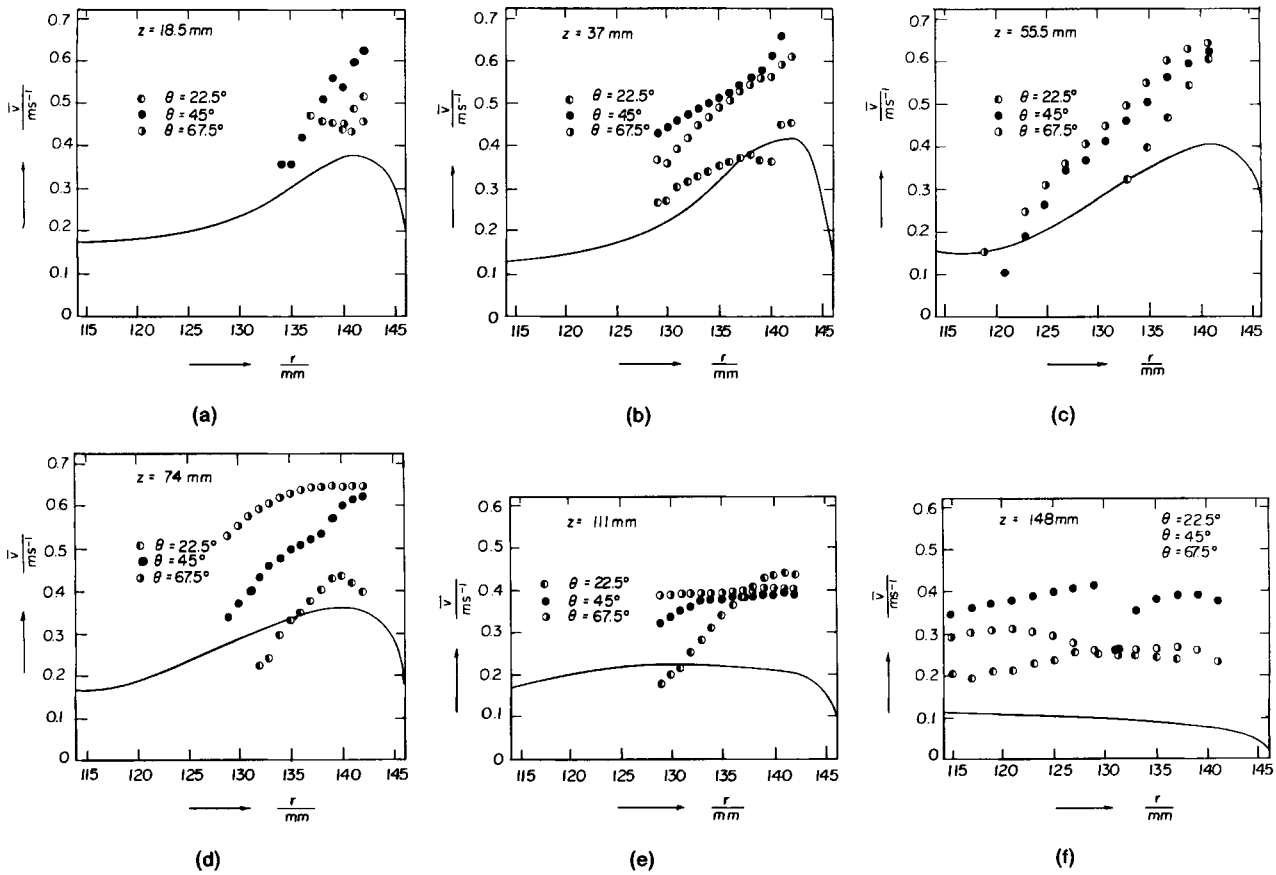

Figure 8. Experimentally determined velocity profiles at tank wall for $T/D = 3$, $N = 400$ min^{-1}.

itself. Second, the velocity profiles measured at the tank wall verify the secondary circulation predicted by the mathematical model. Third, the intensity of turbulence at the tank wall is small compared to that in the impeller discharge flow, while the mean velocity is still high enough to warrant a satisfactory accuracy of measurements. Fourth, and finally, it is of interest to check the results of computations in the region where the assumption of the axial symmetry is mainly violated.

In order to adjust the Pitot tube at the wall properly, it was first necessary to evaluate the vertical deviation of the flow by means of the indication threads. The number of readings at each point was chosen to satisfy the 5% confidence level. Averaged values obtained in this fashion are shown in Figures 5 and 6. The ratio of tangential to axial velocity components is somewhat larger for the smaller impeller ($D = T/4$), with the direction varying remarkably little within the flow field. The only significant differences of the mean directions and their standard deviations appear at the uppermost measured row, at a distance $z =$ 148 mm above the impeller disk plane (i.e., 37 mm under the quiescent water level). The existence of a recirculation vortex at the free level is confirmed by the discontinuities of the measured velocity profiles at $z = 148$ mm in Figures 8 and 9. The discrepancies between the measured and calculated profiles of the mean velocity for $z = 148$ mm are probably caused by modeling the free surface as a *horizontal* plane. The boundary condition used in this model does not express an observed increase in the free surface height at the wall. The indicated presence of the reversed recirculation loop at the free surface therefore must be regarded only as qualitative.

It is of interest to compare the impeller discharge flow rate q_d, defined as the volumetric flow rate through the impeller zone, with the overall tank circulation rate q_c predicted by the numerical solution. The value obtained is $q_c/q_d = 4.1$, which is larger than the value $q_c/q_d = 1.8$–1.9 given by Nagata (1975) for a paddle-impeller agitated system. A similar value $q_c/q_d = 1.96$ was reported by Sachs and Rushton (1954), who used a turbine-type impeller. There are no other available data on the overall circulation rate in the turbine-impeller agitated tanks, and the agreement with the experimental data can be confirmed only by indirect comparison of experimentally determined and computed velocity profiles.

It is also possible to define a circulation time based on the overall tank circulation q_c and the vessel volume by $t = V_t/q_c$. The value of the circulation time provides a good measure of the mean flow for direct comparison with the experimental circulation time correlation of Holmes et al. (1964);

$$t_c = (\tau/N)(T/D)^2 \tag{25}$$

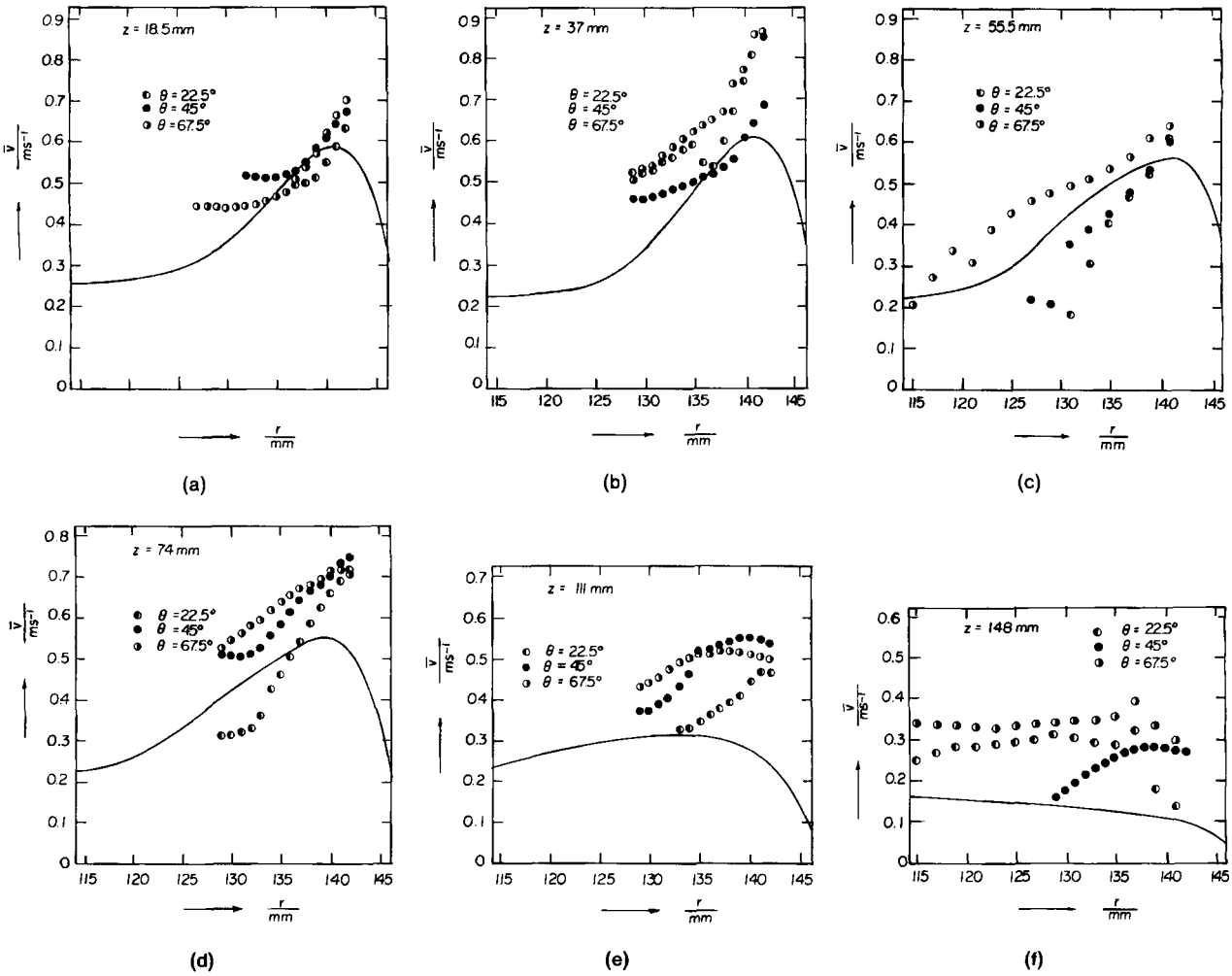

Figure 9. Experimentally determined velocity profiles at tank wall for $T/D = 4$, $N = 840$ min^{-1}.

where τ is a dimensionless group. The experimental measurements of Holmes et al. were made over a wide range of vessel sizes (0.00882 to 0.785 m^3) and turbine speeds (30 to 1,5000 rpm in the 0.0082 m^3 vessel). The dimensionless group τ approaches the constant value 0.85 for impeller Reynolds numbers greater than 20,000. The circulation time from the numerical solution is respectively 1.32 and 1.95 s for $N = 840\ min^{-1}$ and $N = 400\ min^{-1}$. These values compare favorably with the correlated circulation times of $t_c = 0.97$ s and $t_c = 2.04$ s.

From Figures 8 and 9 it follows that the mathematical model overestimates the mean velocity in the impingement region near the impeller disk plane. First, it is noted that the model is two-dimensional and the flow in this region is strongly three-dimensional. Further, additional discrepancies are probably caused by the use of the boundary condition for the equilibrium boundary layer also in the impingement region. The equilibrium between the local production and dissipation of turbulence can hardly be expected in the vicinity of the stagnant point, due to the transport of high-intensity turbulence from the impeller discharge flow. The values of turbulence viscosity predicted by the model therefore are lower than the actual values. The existence of the stagnant point itself is probably restricted only to a small region behind the baffle, as a result of the tangential flow of the fluid. The effort to include the tangential flow at the tank wall into the boundary conditions, Eqs. 14 and 15, resulted in numerical instabilities in the algorithm. Nevertheless, from Figures 8 and 9 it follows that the computed profiles of mean velocity at the tank wall midway between the impeller disk plane and the free surface correspond to the experimental data.

The accuracy of the model is also influenced by the assumption of impeller discharge flow symmetry along the impeller disk plane. The flow in the impeller region is symmetric only for identical lower and upper recirculation loops, i.e., for an agitated system with the impeller positioned at $H/2$, and equipped with an upper deck. Drbohlav et al. (1978) showed that in a commonly used agitated system (as described in the experimental setup), the impeller discharge flow turns slightly to the free surface as a result of the lower hydraulic resistance in the upper recirculation loop. The displacement of the maximum value of the mean velocity from the impeller disk plane was reported equal to $0.05h$. Their data also indicate that horizontal asymmetry of the impeller discharge flow increases in larger vessels.

The computed profile of the tangential component of mean velocity, Figure 10, displays a sharp decrease of $\bar{v}_\theta$ in the impeller region, and almost uniform values in the remaining volume of the tank. The values of $\bar{v}_\theta$ at the tank wall are based on a simple correlation given by Eq. 18. The value of the angle between the axial and tangential components of mean velocity used in Eq. 18 was taken as an average value from Figures 5 and 6. Considering the interval of tangential coordinates: $\theta = 22.5°$, $\theta = 45°$, and $\theta = 67.5°$, Eq. 18 is not valid in close vicinity to the baffles. The computed profiles of $\bar{v}_\theta$ therefore model the fluid flow midway between the two neighboring baffles. Wall temperature profiles published by Strek (1963) also indicate substantial differences in velocities for $\theta = 9°$ and $\theta = 81°$. A similar conclusion follows from variances of the wall shear stress profiles published by Stammers (1969), and from the profiles of the mass transfer coefficient at the tank wall reported by Nagata (1975). The effect of baffles is also included implicitly in the boundary condition for the impeller discharge flow. The generation of the trailing vortices behind the impeller blades is condi-

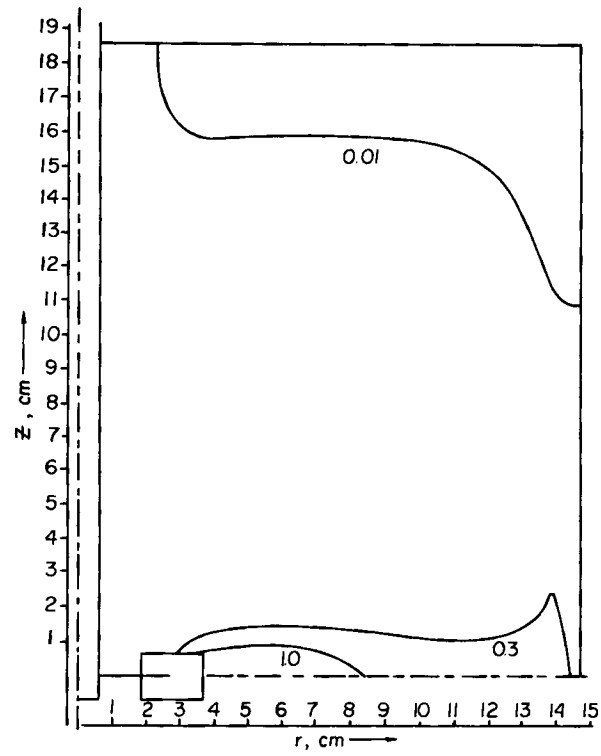

Figure 10. Calculated profiles of tangential component of mean velocity $\bar{v}_\theta$ in ms/s for system in Fig. 4.

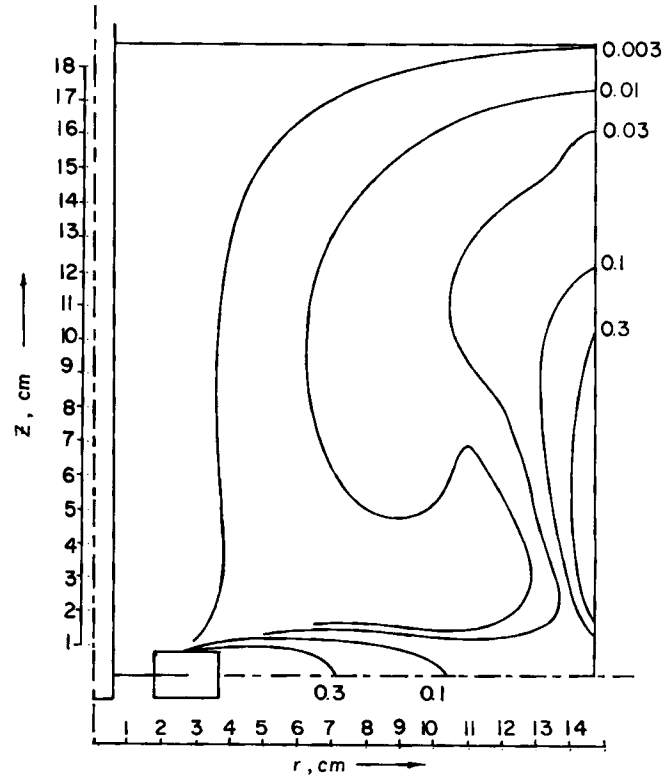

Figure 11. Calculated profiles of overall kinetic energy of turbulence k in m^2s^{-2} for system in Fig. 4.

tioned by a large difference between the tangential velocity component in the impeller inflow region and the circumferential velocity of the impeller. As was shown by Placek and Tavlarides (1985), the rotation of trailing vortices substantially decreases the tangential momentum at the border of the discharge flow. Consequently, such a boundary condition results also in low values of $\bar{v}_\theta$ in the bulk of the tank. On the other hand, in an unbaffled system the value of $\bar{v}_\theta$ at the blade edges is much higher, closer to the circumferential velocity of the impeller (Nagata et al., 1958).

The profile of the overall kinetic energy of turbulence, Figure 11, indicates the convective character of the transport of turbulence in the impeller discharge and wall jet regions. The values of k in the remaining volume of the tank vary relatively little, and some degree of the equilibrium between the rate of production of large-scale turbulence and the rate of its transport to the higher wave-number eddies is acceptable. The individual components making up the overall kinetic energy are indicated by the kinetic energy of large vortices, Figure 12, and the kinetic energy of the transfer eddies, Figure 13.

The profile of the dissipation rate of turbulence, Figure 14, follows from the distribution of turbulence energy. The values of ϵ in the impeller discharge flow and in the impingement region steeply decrease, and they show only one order of magnitude difference in the remaining tank volume. These differences are smaller than those obtained by the use of the simple k-ϵ model: Placek (1980) found one order of magnitude higher difference, while the difference computed by Platzer (1981) is two orders of magnitude higher. A higher degree of homogeneity in the bulk of the tank, obtained by the use of the three-equation model of turbulence, confirms the reliability of the presented model.

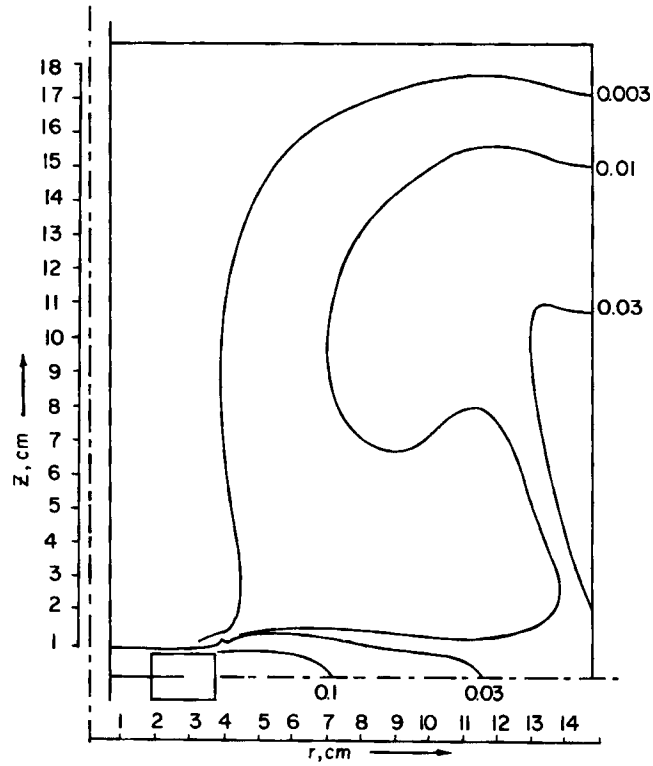

Figure 13. Calculated profiles of kinetic energy of transfer eddies k_T in m^2s^{-2} for system in Fig. 4.

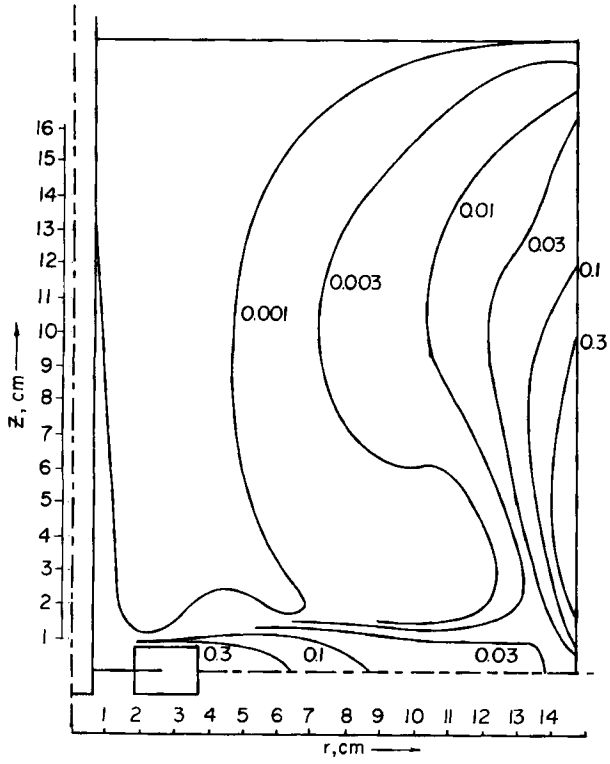

Figure 12. Calculated profiles of kinetic energy of large vortices k_p in m^2s^{-2} for system in Fig. 4.

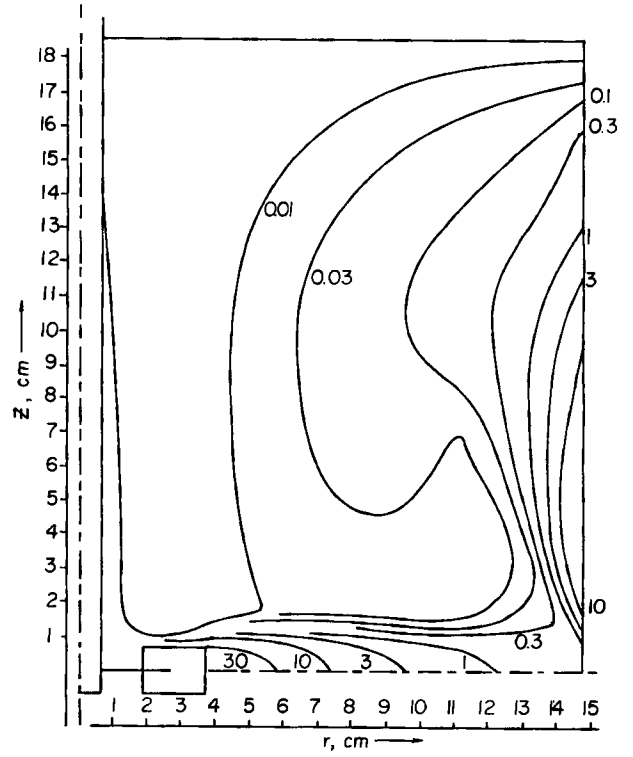

Figure 14. Calculated profiles of dissipation rate of turbulence ϵ in m^2s^{-3} for system in Fig. 4.

The model is being applied to predict mixing of fluids at the microscale level by following tracer experiments. Work is in progress to model nonhomogeneous dispersions undergoing interphase mass transfer and chemical reaction.

Acknowledgment

Financial support provided by the National Science Foundation, Grant Nos. CPE-82-09694 and CPE-84-13869, is gratefully acknowledged.

Notation

A = coefficient in convective terms, Eq. 2
B, C = coefficients in diffusion terms, Eq. 2
b = baffle width
C_D = coefficient in transfer term of turbulence energy, Table 1
C_P = coefficient in production term of dissipation rate of turbulence, Table 1
C_ϵ = coefficient in dissipation term of dissipation rate of turbulence, Table 1
C_λ = coefficient, Eq. 4
C_μ = coefficient in turbulence viscosity term
C_1, C_2 = calibration coefficients, Eq. 19
D = impeller diameter
F = coefficient in substitution formula, Eq. 18
Fc, Fd = convective and diffusion components of F
Fd^* = Fd corrected for the effect of false diffusion, Eq. A11
G = rate of strain
H = quiescent fluid level in tank
h = impeller blade width
k = kinetic energy of turbulence
k_P = kinetic energy of large vortices
k_T = kinetic energy of transfer eddies
ℓ = turbulence length scale
M = ratio of wall and near-wall radii, $M = r_w/r_m$
N = impeller rotational speed
p = pressure
$\overline{p}_{dyn}$ = dynamic pressure measured by Pitot tube
Pe = Peclet number
q_c = tank circulation volumetric flow rate
q_d = impeller discharge volumetric flow rate
R = impeller radius
r = radial coordinate
Re_M = Reynolds mixing number, $Re_M = ND^2/\nu$
S = source term, Eq. 2
Sc = Schmidt number
T = tank diameter
t = instantaneous time or circulation time, V_t/q_c
t_c = correlated circulation time, Eq. 21
u_* = shear velocity, $u_* = (\tau_w/\rho)^{1/2}$
V = volume of finite element
V_t = volume of tank
$\overline{v}$ = mean velocity
x_i = general coordinate
y = distance from tank wall
y^+ = dimensionless distance from tank wall, $y^+ = u_* y/\nu$
z = axial coordinate

Greek letters

α = angle, Eq. 19
Δv = relative error of mean velocity measurement caused by turbulence
δ = relative intensity of turbulence
θ = tangential coordinate
ϵ = dissipation rate of turbulence
θ = general balanced variable
Ψ = stream function
$\overline{\Psi}$ = time-mean stream function
κ = von Kármán constant, $\kappa = 0.41$
Λ = macroscale of turbulence
μ = dynamic viscosity
ν = kinematic viscosity
ρ = density
τ = dimensionless circulation time, Eq. 21
τ_w = wall shear stress
ω = vorticity
$\overline{\omega}$ = time-mean vorticity

Subscripts

eff = effective value
k = kinetic energy
m = grid node once removed from wall
r = radial component
t = turbulent
w = wall value
z = axial component
ϵ = turbulence dissipation
θ = tangential component

Literature cited

Ambegaonkar, A. S., A. S. Dhruv, and L. L. Tavlarides, "Fluid-Particle Hydrodynamics in Agitated Vessels," *Can. J. Chem. Eng.*, **55,** 414 (1977).

Bradshaw, P., T. Cebecci, and J. H. Whitelaw, *Engineering Calculation Methods for Turbulent Flow,* Academic Press (1981).

Cantwell, B. J., "Organized Motion in Turbulent Flow," *Ann. Rev. Fluid Mech.*, **13,** 457 (1981).

Cutter, L. A., "Flow and Turbulence in a Stirred Tank," *AIChE J.*, **12,** 35 (1966).

Danon, H., M. Wolfshtein, and G. Hetsroni, "Numerical Calculations of Two-Phase Turbulent Round Jet," *Int. J. Multiphase Flow,* **3,** 223 (1977).

DeSouza, A., and R. W. Pike, "Fluid Dynamics and Flow Patterns in Stirred Tanks with a Turbine Impeller," *Can. J. Chem. Eng.*, **50,** 15 (1972).

Drbohlav, J., I. Fořt, K. Máca, and J. Ptáček, "Turbulent Characteristics of Discharge Flow from the Turbine Impeller," *Coll. Czech. Chem. Commun.*, **43,** 3148 (1978).

Escudier, M. P., "The Distribution of Mixing Length in Turbulent Flows Near Walls," Report TWF/IN/1, Heat Transfer Sec., Imperial Coll. Sci. Tech., London (1966).

Folsom, R. G., "Review of the Pitot Tube," *Trans. ASME,* **78,** 1447 (1956).

Fořt, I., M. Hrach, and A. Obeid, "Flow into the Standard Impeller Region in the Cylindrical System with Radial Baffles," (in Czech), *Sci. Papers Prague Inst. Chem. Technol.*, **K15,** 37 (1980).

Fořt, I., H. O. Möckel, J. Drbohlav, and M. Hrach, "The Flow of Liquid in a Stream from the Standard Turbine Impeller," *Coll. Czech. Chem. Commun.*, **44,** 700 (1979a).

Fořt, I., A. Obeid, and V. Březina, "Flow of Liquid in a Cylindrical Vessel with a Turbine Impeller and Radial Baffles," *Coll. Czech. Chem. Comm.*, **47,** 226 (1982).

Fořt, I., J. Placek, F. Strek, Z. Jaworski, and J. Karcz, "Heat and Momentum Transfer in the Wall Region of a Cylindrical Vessel Mixed by a Turbine Impeller," *Coll. Czech. Chem. Commun.*, **44,** 684 (1979b).

Fořt, I., J. Podivínská, and R. Baloun, "The Study of Convective Flow in a System with a Rotary Mixer and Baffles," *Coll. Czech. Chem. Commun.*, **34,** 959 (1969).

Gosman, A. D., W. M. Pun, A. K. Runchal, D. B. Spalding, and M. Wolfshtein, *Heat and Mass Transfer in Recirculating Flows,* Academic Press (1969).

Günkel, A. A., and M. E. Weber, "Flow Phenomena in Stirred Tanks," *AIChE J.*, **21,** 931 (1975).

Hanjalic, K., B. E. Launder, and R. Schiestel, "Multiple-Time-Scale Concepts in Turbulent Transport Modeling," *Lec. Ser.* 1980–3, **I,** von Karman Inst. Fluid Dynamics, Rhode Saint Genese, (1980).

Harvey, P. S., and M. Greaves, "Turbulent Flow in an Agitated Vessel," *Trans. Inst. Chem. Eng.*, **60,** 195 (1982).

Hinze, J. O., *Turbulence,* McGraw Hill & Co., Inc., New York (1975).

Holmes, D. B., R. M. Voncken, and J. A. Dekker, "Fluid Flow in Turbine Stirred Baffled Tanks. I: Circulation Time," *Chem. Eng. Sci.*, **19,** 201 (1964).

Hussain, A. K. M. F., "Coherent Structures—Reality or Myth?" *Physics of Fluids*, **26**, 2816 (1983).
Kitaura, Y., Y. Nagase, M. Kakumoto, and T. Haseqawa, "Effect of Pitot Tube on the Result of Measurement of Velocity Distribution in an Agitated Vessel," (in Japanese), *Kagaku Kogaku*, **36**, 1152 (1970).
Komasawa, I., R. Kuboi, and T. Otake, "Fluid and Particle Motion in Turbulent Dispersion. I," *Chem. Eng. Sci.*, **29**, 641 (1974).
Launder, B. E., and D. B. Spalding, *Mathematical Models of Turbulence*, Academic Press (1972).
———, "The Numerical Computation of Turbulent Flow," *Comp. Meth. Appl. Mech. Eng.*, **3**, 269 (1974).
Lelan, A., and H. Angelino, "Etude d'une cuve agitee munie de chicanes: Transfert de matiere a une sphere fixe," *Chem. Eng. Sci.*, **29**, 907 (1974).
Ljuboja, M., and W. Rodi, "Calculation of Turbulent Wall Jets with an Algebraic Reynolds Stress Model," *Trans. ASME, J. Fluids Eng.*, **102**, 350 (1980).
Mujumdar, A. S., B. Huang, D. Wolf, M. E. Weber, and W. J. M. Douglas, "Turbulence Parameters in a Stirred Tank," *Can. J. Chem. Eng.*, **48**, 519 (1970).
Nagase, Y., T. Yoshida, T. Iwamoto, and S. Fujita, "On Flow Characteristics in Stirred Tank with Paddle-Type Impeller," (in Japanese), *Kagaku Kogaku*, **38**, 519 (1974).
Nagata, S., *Mixing—Principles and Application*, Halsted Press, Wiley, New York, pp. 134–136, 158, 165 (1975).
Nagata, S., K. Yamamoto, K. Hashimoto, and Y. Naruse, "Flow Patterns of Liquids in a Cylindrical Mixing Vessel with Baffles," *Mem. Fac. Eng., Kyoto Univ.*, **21**, 60 (1969).
Nagata, S., K. Yamamoto, and M. Ujihara, "Flow Patterns of Liquids in a Cylindrical Mixing Vessel without Baffles," *Mem. Fac. Eng., Kyoto Univ.*, **20**, 336 (1958).
Nielsen, H. J., "Flow and Turbulence from a Flat-Blade Turbine Mixing Impeller," Ph.D. Thesis, Ill. Inst. Tech., Chicago (1958).
Okamoto, Y., M. Nishikawa, and K. Hashimoto, "Energy Dissipation Rate Distribution in Mixing Vessels and its Effects on Liquid-Liquid Mass Transfer," *Int. Chem. Eng.*, **21**, 88 (1981).
Patankar, S. V., *Numerical Heat Transfer and Fluid Flow*, Hemisphere (1980).
Placek, J., "A Numerical Solution of Non-Newtonian Flow Equations for Mixing Apparatuses," (in Czech), *Proc. 3rd Conf. Indust. Rheology*, Otrokovice (1978).
———, "The Hydrodynamics of a Mechanically Agitated System," (in Czech), Ph.D. Thesis, Czech. Acad. Sci., Inst. Microbiol., Prague (1980).
Placek, J., I. Fořt, F. Strek, Z. Jaworski, and J. Karcz, "Velocity Field at the Wall of Fully Baffled Vessel with a Turbine Impeller," *Proc. 5th Cong. CHISA*, Prague (1978).
Placek, J., and L. L. Tavlarides, "Turbulent Flow in Stirred Tanks. I: Turbulent Flow in the Turbine Impeller Region," *AIChE J.*, **31**, 1113 (July, 1985).
Platzer, B., "A Contribution to the Evaluation of Turbulent Flow in Baffled Tanks with Radial Outflow Impellers," (in German), *Chem. Technik*, **33**, 16 (1981).
Platzer, B. and G. Noll, "An Analytical Solution for the Flow in Baffled Vessels with Radial Outflow Impellers," (in German), *Chem. Technik*, **33**, 648 (1981).
Rao, M. A., and R. S. Brodkey, "Continuous-Flow Stirred-Tank Turbulence Parameters in the Impeller Stream," *Chem. Eng. Sci.*, **27**, 137 (1972).
Rodi, W., *Turbulence Models and Their Applications in Hydraulics—A State of the Art Review*, Int. Ass. Hydraulic Res., Delft, Netherlands (1980).
Sachs, J. P., and J. H. Rushton, "Discharge Flow from Turbine-Type Mixing Impellers," *Chem. Eng. Prog.*, **50**, 597 (1954).
Schwartzberg, H. G., and R. E. Treybal, "Fluid and Particle Motion in Turbulent Stirred Tanks," *Ind. Eng. Chem. Fundam.*, **7**, 1 (1968).
Stammers, F. "Local Heat Transfer Coefficients in Stirred Vessels," (in Flemish), Ph.D. Thesis, Tech. Univ. Delft, Netherlands (1969).
Strek, F. "Heat Transfer in Liquid Mixers, Study of a Turbine Agitator with Six Flat Blades," *Int. Chem. Eng.*, **3**, 533 (1963).
Thiele, H., "Flow and Power Input in Mixing of Newtonian Fluids: Anchor, Paddle and Turbine Impellers in Laminar Region," (in German), Ph.D. Thesis, Tech. Univ. Berlin, West Berlin (1972).
van't Riet, K., "Turbine Agitator Hydrodynamics and Dispersion Performance," Ph.D. Thesis, Tech. Univ. Delft, Netherlands (1975).
van't Riet, K., and J. M. Smith, "The Trailing Vortex System Produced by Rushton Turbine Agitators," *Chem. Eng. Sci.*, **30**, 1093 (1975).
van't Riet, K., W. Bruijn, and J. M. Smith, "Real and Pseudo-Turbulence in the Discharge Stream from a Rushton Turbine," *Chem. Eng. Sci.*, **15**, 407 (1976).
Wolfshtein, M., "Convection Processes in Turbulent Impinging Jets," Ph.D. Thesis, Report SF/R/I/2, Heat Transfer Sec., Imperial Coll. Sci. Tech., London (1967).
Yamamoto, K., and S. Nagata, "Analytical Studies on the Flow Patterns of Liquid in a Cylindrical Mixing Vessel," (in Japanese), *Kagaku Kogaku*, **26**, 500 (1962).

Manuscript received Nov. 30, 1983, and revision received Mar. 31, 1986.

See NAPS document no. 04422 for 6 pages of supplementary material. Order from NAPS c/o Microfiche Publications, P.O. Box 3513, Grand Central Station, New York, NY 10163. Remit in advance in U.S. funds only $7.75 for photocopies or $4.00 for microfiche. Outside the U.S. and Canada, add postage of $4.50 for the first 20 pages and $1.00 for each of 10 pages of material thereafter, $1.50 for microfiche postage.